# EVALUATION OF A REACTIVE-HEAT-PIPE EMPLOYING AN ARTERIAL WICK

Technical Report

Sponsored by

Prepared by
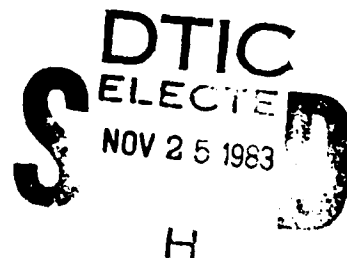
G. A. Szekely and G. M. Faeth

The Pennsylvania State University
College of Engineering
Department of Mechanical Engineering
University Park, Pennsylvania

June 1978

83 11 25 012

EVALUATION OF A REACTIVE-HEAT-PIPE
EMPLOYING AN ARTERIAL WICK

Technical Report
June 1978

The views and conclusions contained in this document are those
of the authors and should not be interpreted as necessarily
representing the official policies, either expressed or implied,
of the Advanced Research Projects Agency of the U. S. Government.

Prepared by

G. A. Szekely and G. M. Faeth

Telephone (814) 865-3743

Mechanical Engineering Department
The Pennsylvania State University
University Park, Pennsylvania 16802

| Accession For | |
| --- | --- |
| NTIS GRA&I | ☑ |
| DTIC TAB | ☐ |
| Unannounced | ☐ |
| Justification | |
| By | |
| Distribution/ | |
| Availability Codes | |
| Dist | Avail and/or Special |
| A -1 | |

| REPORT DOCUMENTATION PAGE | | READ INSTRUCTIONS BEFORE COMPLETING FORM |
|---|---|---|
| 1. REPORT NUMBER | 2. GOVT ACCESSION NO. <br> AD - P134924 | 3. RECIPIENT'S CATALOG NUMBER |
| 4. TITLE (and Subtitle) <br><br> Evaluation of a Reactive-Heat-Pipe Employing an Arterial Wick | | 5. TYPE OF REPORT & PERIOD COVERED <br> Interim |
| | | 6. PERFORMING ORG. REPORT NUMBER |
| 7. AUTHOR(s) <br><br> G. A. Szekely and G. M. Faeth | | 8. CONTRACT OR GRANT NUMBER(s) <br><br> N00600-74-C-0033 |
| 9. PERFORMING ORGANIZATION NAME AND ADDRESS <br><br> Department of Mechanical Engineering <br> The Pennsylvania State University <br> University Park, Pennsylvania 16802 | | 10. PROGRAM ELEMENT, PROJECT, TASK AREA & WORK UNIT NUMBERS <br><br> 62105E, 2N10 <br> Other DOD-ARPA, 2724-510-50 |
| 11. CONTROLLING OFFICE NAME AND ADDRESS <br><br> Defense Advanced Research Projects Agency <br> 1400 Wilson Blvd., Arlington, VA 22209 | | 12. REPORT DATE <br> June 1978 |
| | | 13. NUMBER OF PAGES |
| 14. MONITORING AGENCY NAME & ADDRESS(if different from Controlling Office) <br> David W. Taylor, Naval Ship R & D Center <br> Annapolis, MD 21402 | | 15. SECURITY CLASS. (of this report) <br> U |
| | | 15a. DECLASSIFICATION/DOWNGRADING SCHEDULE |
| 16. DISTRIBUTION STATEMENT (of this Report) <br><br> Approved for Public Release; distribution unlimited | | |
| 17. DISTRIBUTION STATEMENT (of the abstract entered in Block 20, if different from Report) | | |
| 18. SUPPLEMENTARY NOTES | | |
| 19. KEY WORDS (Continue on reverse side if necessary and identify by block number) <br><br> Liquid Metal Combustor; Liquid Metal Reactor | | |

20. ABSTRACT (Continue on reverse side if necessary and identify by block number)

This report describes a theoretical and experimental study of the use of arterial wicks in conjunction with a reactive-heat-pipe combustor for the lithium-sulfurhexafluoride reactant combination. The theory suggests substantial increases in allowable wick power densities (to levels on the order of $MW/m^2$) when arterial wicks are used, improving the compactness of the combustor system.

(continued on next page)

Tests were conducted to determine maximum wick power densities. A 15 kW combustor was used, employing two arterial wick assemblies with a design power density of $4MW/m^2$. The results indicated only a small improvement of the maximum power density over conventional wicks (310-440 $kW/m^2$). The findings suggest that combustion rates were very nonuniform over the wick surface for this test configuration. The use of wick designs with a smaller aspect ratio is proposed as a method of avoiding the nonuniform combustion problem in order to achieve the full potential of the arterial wick configuration.

Evaluation of a Reactive-Heat-Pipe Employing an Arterial Wick

## Summary

This investigation is considering the development of combustor systems based on the chemical reaction between gaseous sulfurhexafluoride and molten lithium. This reactant combination has a high energy density on both a weight and volume basis, and the products of reaction are condensed materials which do not have to be exhausted to the ambient environment. These characteristics make the liquid metal combustor system desirable for use as the heat source of underwater power systems using closed thermodynamic cycle, e.g. Brayton, Ranskine, Stirling cycle, etc.

The objective of the investigation is to develop a combustor system which can operate for long durations with variable thermal output. The combustor must be capable of shutdown and restarting, refueling, and totally sealed operation.

Earlier work established the reactive-heat-pipe as the most promising concept for meeting these objectives. It was also suggested that the use of arterial wicks could improve the performance of reactive-heat-pipes over conventional wicks. This report describes the results of an investigation of the arterial wick concept.

The investigation was divided into theoretical and experimental phases, the results of each phase of the study may be summarized as follows:

1. Analysis

   Theoretical models were constructed to determine the self-priming and wick pumping capabilities of arterial wicks. It was found that 1mm diameter arteries would be capable of self-priming to the height required for experimental purposes with an adequate factor of safety. Auxiliary tests were conducted which substantiated the self-priming predictions.

   The use of arterial wicks results in a substantial increase in allowable wick power densities, without wick dryout. It appears that arterial wicks are capable of wick power densities on the order of $MW/m^2$, providing real potential for compact combustor systems. In these circumstances, the displacement of liquid at the base of the wick, due to the temperature and thus vapor pressure difference across the wick, becomes the limiting factor in reactive-heat-pipe design, tending to limit allowable wick power densities.

2. Experiments

   Based on the analysis, arterial wick assemblies were designed for use with the 15kW reactive-heat-pipe combustor employed in earlier testing. The combustor employs two injector/wick assemblies. The arterial arrangement involved the use of four 1mm diameter arteries, equally spaced around the periphery of each wick. With this arrangement, the wick pumping capability was predicted to be $4MW/m^2$.

The arterial wick configuration was tested to determine maximum wick power densities at wick burnout conditions. The tests indicated a relatively small improvement of the maximum power density over the conventional wick, in spite of the improved pumping capability of the wick (burnout conditions involved wick power densities of $310-440kW/m^2$). This result suggests that burnout is due to very nonuniform combustion rates over the wick surface, perhaps involving deflection of the oxidizer jet on to the surface of the wick. The design change needed to avoid this problem involves reducing the aspect ratio (height/diameter) of the wick assembly. Further experiments are required to test this possibility; however, if this approach is successful arterial wicks could provide very compact combustor configurations.

## Acknowledgements

## TABLE OF CONTENTS

vii

## LIST OF TABLES

| Table | Title | Page |
|---|---|---|
| 1 | Standard wick configuration . . . . . . . . . . . . . . | 11 |
| 2 | Maximum artery sizes for self-priming . . . . . . . . . | 12 |
| 3 | Comparison of predictions with the two property models | 13 |
| 4 | Effect of mean temperature on maximum wick power density . . . . . . . . . . . . . . . . . . . . . . . | 14 |
| 5 | Effect of liquid displacement on maximum wick power density . . . . . . . . . . . . . . . . . . . . . . . | 15 |
| 6 | Effect of number and diameter of arteries on maximum wick power density . . . . . . . . . . . . . | 17 |
| 7 | Comparison of conventional and arterial wicks . . . . . | 18 |
| 8 | Summary of self-priming test results . . . . . . . . . | 22 |
| 9 | Design summary of the reactive-heat-pipe employing arterial wicks. . . . . . . . . . . . . . . . . . . . . | 25 |
| 10 | Summary of arterial wick reactive-heat-pipe combustor test . . . . . . . . . . . . . . . . . . . . . . . . . | 29 |

## LIST OF FIGURES

## NOMENCLATURE

| Symbol | Description |
|--------|-------------|
| A | area |
| $d_a$ | artery diameter |
| $d'$ | wire diameter of screen |
| f | Moody friction factor |
| g | gravitational acceleration |
| h | self-priming height |
| $h_{fg}$ | heat of vaporization |
| H | wick height |
| K | wick permeability |
| L | liquid surface displacement |
| $L_a$ | crossectional artery length |
| $\dot{m}$ | mass flow rate |
| $\dot{m}''$ | mass flux |
| N | mesh size |
| $\dot{q}''$ | heat flux |
| $Q_r$ | heat of reaction |
| R | meniscus radius |
| Re | Reynolds number |
| s | artery spacing |
| t | wick thickness |
| $W_a$ | crossectional width of artery |
| y | distance from top of wick |

## NOMENCLATURE (continued)

| Symbol | Description |
|---|---|
| $\alpha$ | parameter, Eq. (3-5) |
| $\delta$ | wire spacing |
| $\epsilon'$ | wick void fraction |
| $\theta$ | artery angle |
| $\mu$ | viscosity |
| $\rho$ | density |
| $\sigma$ | surface tension |

Subscripts

| | |
|---|---|
| A, B, C, D | positions in Fig. 1 |
| f | viscous |
| g | gravitational |
| max | maximum value |
| o | bottom of wick |
| W | wick |

## Evaluation of a Reactive-Heat-Pipe Employing an Arterial Wick

Technical Report
June 1978

## 1. Introduction

### 1.1 General Objectives

This investigation is considering the development of a combustor-heat transport system utilizing the chemical reaction between molten lithium and gaseous sulfurhexafluoride. This reaction has a high energy density and the volume of the combustion products is approximately equal to the original volume of the lithium. Therefore, reaction products do not have to be exhausted from the system and the combustor can operate closed. Due to these operating characteristics, the $Li-SF_6$ combustor system is particularly attractive as a thermal energy source for closed heat-power cycles (Rankine, Brayton, etc.) which generate mechanical power for underwater applications.

The successful operation of the $Li-SF_6$ combustor for short periods (less than 1h), in conjunction with a power cycle, has been established in earlier work. The objective of the present investigation is to develop a combustor system capable of long term operation, over a variable thermal load, with periods of total shut-down followed by restart after a storage period of arbitrary length. References 1-9 are earlier reports describing various aspects of the study.

Previous work has established that the reactive-heat-pipe concept is a promising approach toward meeting program objectives [4-6, 9]*. This arrangement involves burning the lithium from one side of a wick in a gaseous environment fed with $SF_6$. The other side of the wick is used as the evaporator of a heat pipe, transporting the reaction energy to the load heat exchanger of the closed power cycle. Prior studies have demonstrated the feasibility of this arrangement [5, 6, 9]. It was also concluded that the use of an arterial wick would allow operation of the system at high power densities than conventional wicks, increasing the compactness of the combustor.

The present investigation examines the use of arterial wicks for the reactive-heat-pipe combustor in more detail. Theoretical analysis was completed to determine the operating limitations of the arterial arrangement, and to indicate the quantitative improvement of system performance over convention wicks. Tests were conducted to demonstrate the feasibility of the concept. This report considers both aspects of the study.

---

* Numbers in brackets designate references at end of report.

In the following, a description of the reactive-heat-pipe concept is
provided, prior to discussing the analysis and the theoretical results.
The report concludes with a description of the experimental arrangement
and a discussion of the experimental results.


## 2. Reactive-Heat-Pipe Concept

The reactive-heat-pipe concept is discussed in some detail, elsewhere
[5, 6, 9]. Only a brief discussion of the system will be presented in the
following, with emphasis on artery arrangements.

A schematic diagram of the reactive-heat-pipe appears in Fig. 1. The
wick is free-standing, mounted at the top of the combustor and sealed at the
bottom with the molten lithium fuel. The products accumulate at the bottom
of the combustor, as a liquid layer which is immiscible with lithium [3, 8].
The $SF_6$ enters the region enclosed by the wick, through an injector. The rate
of reaction is controlled by the rate of inflow of $SF_6$. Reaction can continue
until all the lithium is consumed, at which time, the lower part of the combustor
is filled with molten product to about the same level as the original lithium.

Reaction occurs as a diffusion flame near the surfact of the wick [4].
Lithium passes up the wick by capillary action and evaporates from the inside
surface. After diffusion to the flame zone, the lithium reacts to form products,
releasing chemical energy. The products diffuse back to the wick, where
they condense as droplets (since the liquids are immiscible). The product
droplets drain down the wick and accumulate in the product layer. The product
drops cover only about 10% of the wick surface area, so that lithium evaporation
is relatively unimpeded by the presence of product condensate [4].

The exterior portion of the wick acts as the evaporator of a heat pipe.
Reaction energy is transported to the wick by convection, radiation and product
condensation. The heat is conducted through the wick, causing lithium to
evaporate from the outside surface. The lithium vapor flows to the cooler
heat exchanger surfaces and condenses, transferring the energy of reaction to
the load. The condensate drains back into the lithium bath to complete the
heat pipe cycle.

Since the temperature decreases through the wick, the lithium vapor
pressure difference across the wick causes the liquid level to be displaced
in the region enclosed by the wick. At typical operating temperatures (1200 K),
the lithium vapor pressure is low (on the order of 1kPa) and the liquid
displacement is relatively small (10-20 mm).

The lithium for both reaction and heat-pipe action must pass up the
crossection of the wick. At high power densities, the viscous pressure drop
of the flow through the wick can exceed available capillary forces. This
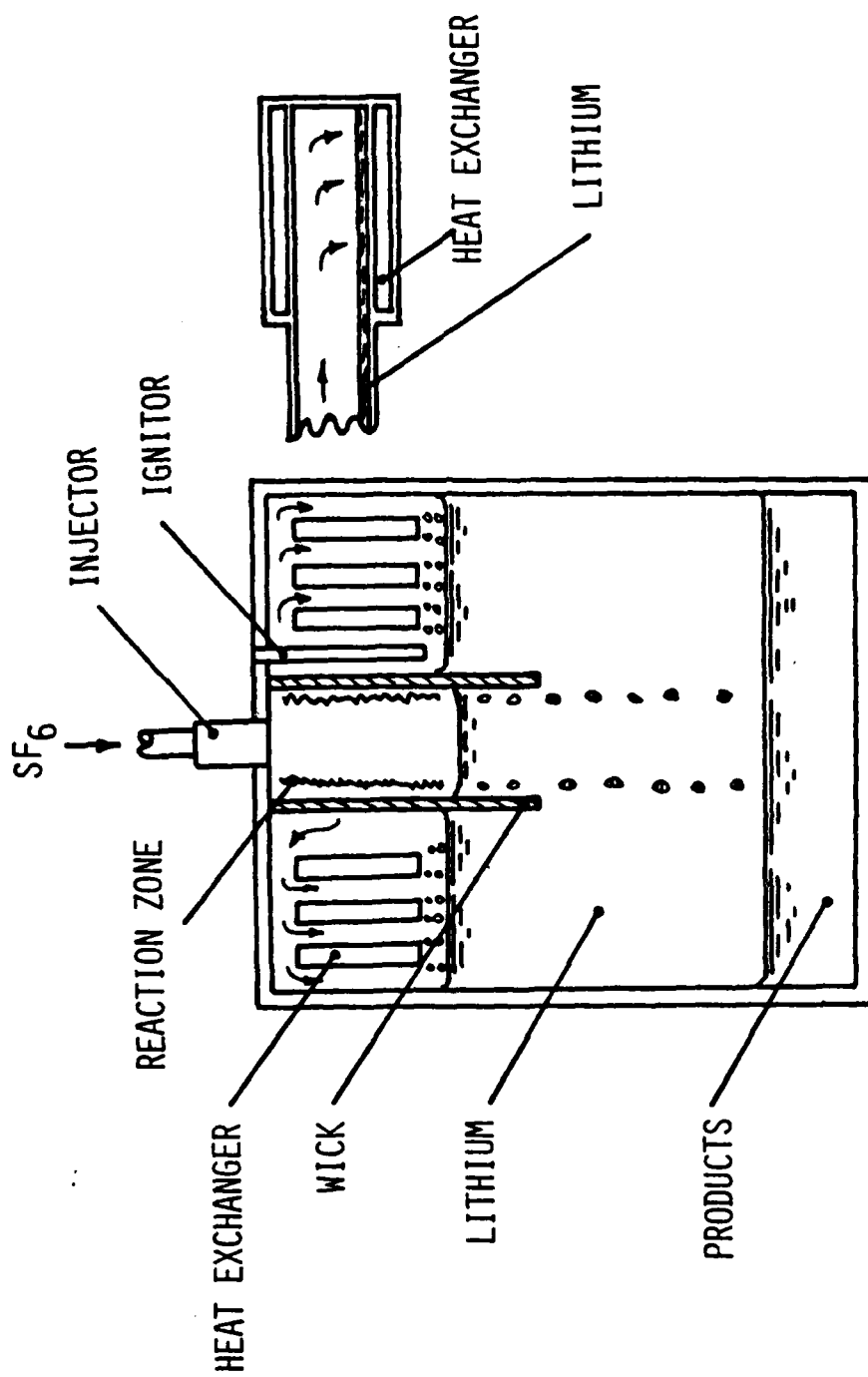causes the top of the wick to dry-off, resulting in wick burnout by direct

Figure 1  Reactive-Heat-Pipe Combustor Concept

corrosion of the wick material (which is stainless steel mesh) by the oxidizer. Nonuniform reaction rates over the surfact of the wick can also cause wick burnout by dryout of local regions of high reaction rates. This behavior was observed in earlier reactive-heat-pipe test at wick heat fluxes greater than 300kW/sgm [6].

One approach that can be taken to increase allowable wick power densities, without dryout, is to increase the thickness of the wick. This provides more flow area for the lithium, reducing the viscous pressure drop. The difficulty with this approach is that increased wick thicknesses result in larger temperature, and thus pressure, differences across the wick. This causes an excessive liquid displacement under the wick area allowing the oxidizer to bubble under the lower edge of the wick, defeating the heat-pipe action.

A more attractive approach for operation at higher power density is to employ an arterial wick, which is a conventional method for increasing the power density of heat pipes [10]. A crossection of an arterial wick for the reactive-heat-pipe is illustrated in Fig. 2. The arteries are spaced around the outside surface of the wick, increasing the crossectional area for flow, without significantly increasing the thickness of the wick. This reduces the viscous pressure drop in the wick without increasing the liquid displacement. A similar arterial wick arrangement is considered in the following theoretical and experimental investigation.


## 3. Theory

The theoretical analysis addresses the requirements for self-priming the wick arteries, and the pumping capabilities of the arterial wick. The characteristics of conventional wicks, the vapor transport system, and condensation on the load heat exchanger, have been considered in earlier work [5].

### 3.1 Self-Priming of Arteries

A requirement of conventional artery design is that the arteries must be self-priming, i.e., sufficient capillary action must be present to draw the liquid to the top of the artery without any unusual manipulation of the combustor, tipping, etc. This is an obvious safety feature so that if the artery does lose priming, e.g., by the formation of a vapor bubble during heatup, it can reprime itself without outside intervention. Self-priming also simplifies wick replacement, since a clean wick can be installed in the combustor without saturating it with lithium beforehand.

Capillary rise occurs because the pressure on the inner surface is less than the outer surface. This pressure difference, is related to the surface tension and the dimensions at the passage in which the capillary rise is occuring. The maximum self-priming height can be determined by neglecting the liquid motion, and simply equating the surface tension forces generated in the artery to the hydrostatic head of the primed artery [10]. In the present arrangement, the artery is vertical.
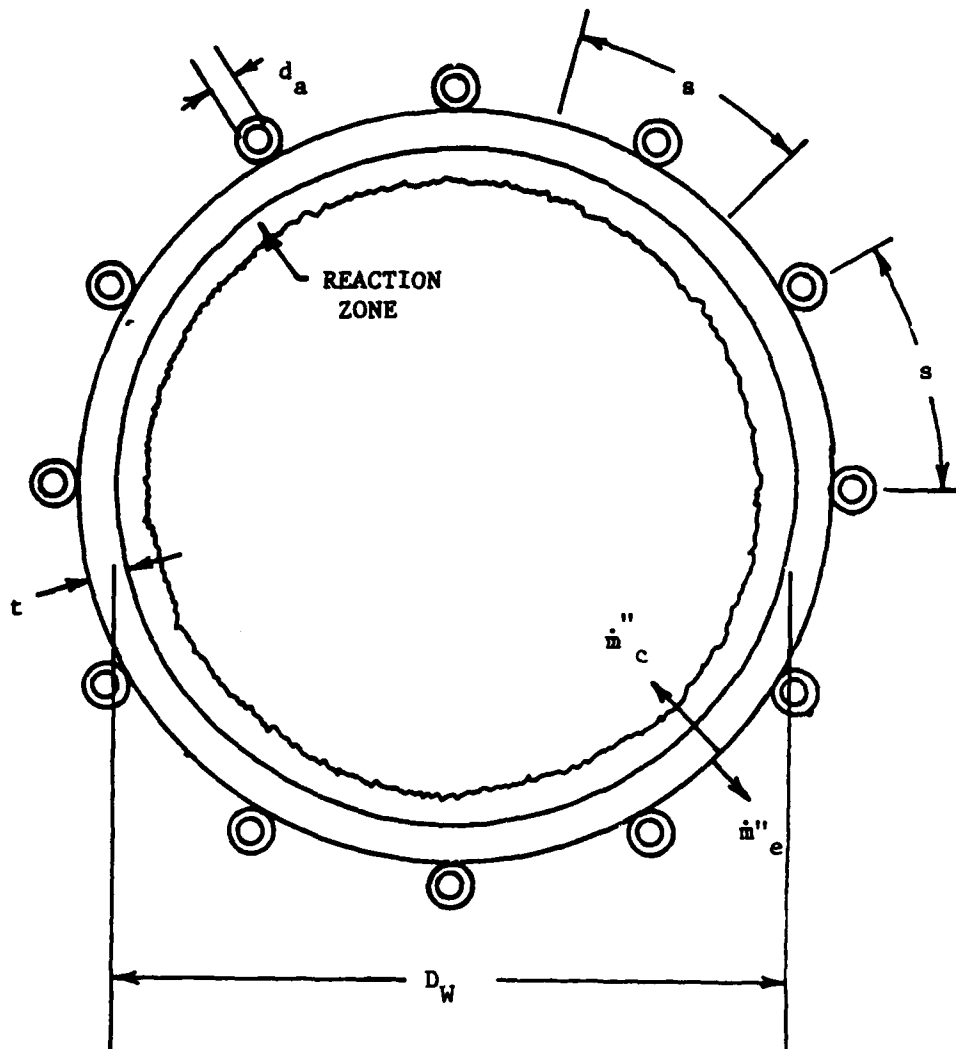
Figure 2  Crossection of the arterial wick

Two different artery crossections are considered, a rectangular artery having dimensions $W_a$, $L_a$, and a circular artery having a diameter $d_a$. The surface tension force acting around the periphery of the rectangular artery is $2(L_a + W_a)\sigma\cos\theta$, where $\theta$ is the contact angle between the fluid and the wall of the artery. The pressure difference across the liquid surface by virtue of the capillary rise in the artery is $\rho gh$ where h is the vertical rise. Equating the surface tension force to the force resulting from the pressure difference, yields the following equation for the capillary rise height:

$$ h = \frac{2\sigma}{\rho g}\left(\frac{1}{L_a} + \frac{1}{W_a}\right)\cos\theta \qquad (3.1) $$

If the liquid is assumed to perfectly wet the wall, $\cos\theta = 1$ [10]. Proceeding in the same manner for the circular artery, the capillary rise height is:

$$ h = 4\sigma/\rho g d_a \qquad (3-2) $$

Equations (3-1) and (3-2) provide the needed design equations. Given the properties of the fluid and the required self-priming vertical rise, h, the artery dimensions can be selected.

## 3.2 Wick Analysis

From symmetry considerations, a section of wick with an artery passing up the center can be analyzed. Figure 3 is a sketch of the model arrangement. The wick has a length H-L above the liquid surface, where L is determined by the temperature difference across the wick, as noted earlier. The parameter s is the spacing between arteries.

For lack of better information, we assume that the rate of reaction is uniform over the inner surface of the wick [5, 6, 9]. All the heat generated by reaction is assumed to pass through the region of the wick above the liquid surface (this is conservative, since some energy is transported to the bath in the displaced region). We also assume that the vertical flow of liquid is confined to the arteries, so that the liquid passes up the artery and then spreads horizontally across the wick. This latter assumption neglects the vertical flow in the wick itself, and is also conservative.

The total mass flux of fuel leaving the wick surface for both combustion and heat transport is:

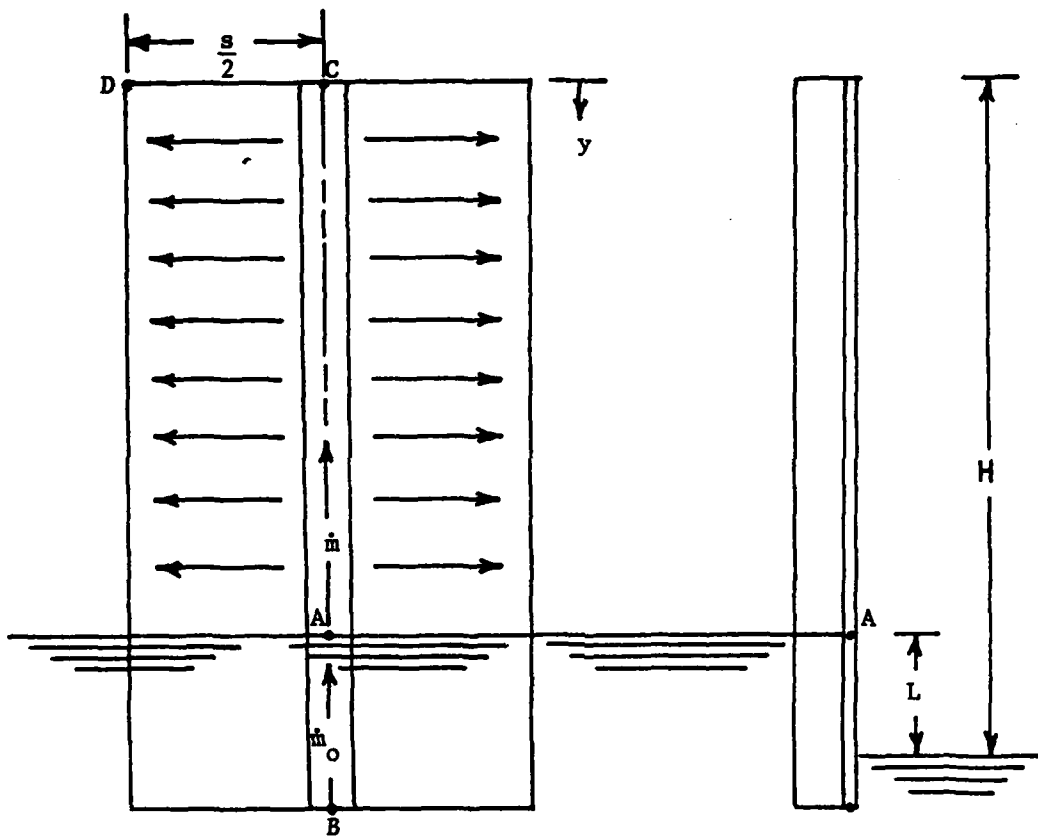$$ \dot{m}'' = \dot{m}''_e + \dot{m}''_c \qquad (3-3) $$

Figure 3  Sketch of a wick segment

The mass fluxes can be expressed in terms of the heat flux through the exposed portion of the wick, as follows:

$$\dot{m}_e'' = \dot{q}''/h_{fg}, \quad \dot{m}_c'' = \dot{q}'' \, (H-L)/HQ_r \qquad (3\text{-}4)$$

applying the assumption that heat is only transferred through the completely exposed portion of the wick. Therefore, the *total flow of* lithium entering an artery is

$$\dot{m}_o = \frac{\dot{q}''Hs}{Q_r} \left[ (1 - \frac{L}{H})(1 + \alpha - \frac{L}{H}) \right] \qquad (3\text{-}4a)$$

where

$$\alpha = Q_r/h_{fg} \qquad (3\text{-}5)$$

For lithium, $\alpha = 2.2$, over the typical operating range of Li-SF$_6$ combustors [5]. The mass flow rate through the artery varies linearly with distance above the liquid surface

$$\dot{m} = \dot{m}_o y/(H-L) \qquad (3\text{-}6)$$

In order for liquid to reach all points on the wick, the available capillary pressure force must be greater than the viscous and hydrostatic pressure drops

$$\Delta p_s \geq \Delta p_f + \Delta p_g \qquad (3\text{-}7)$$

Examination of Fig. 3 indicates that point D is the most critical wick position, since the length of the flow path and height above the liquid surface is greatest for this position. It is assumed that the liquid has ready access to point A at the liquid surface, therefore only the pressure drops between points A and D need be considered.

The viscous pressure gradient in the artery (A-C) is given by [10]

$$\frac{dp}{dy} = \frac{8f\dot{m}^2}{\pi^2 \rho d_a^3} \qquad (3\text{-}7a)$$

The flow in the artery is laminar for conditions considered in this study, therefore

$$f = 64/Re \qquad (3\text{-}8)$$

where

$$Re = 4\dot{m}/\pi\mu d_a \tag{3-9}$$

Substituting Eqs. (3-4a), (3-6), (3-8) and (3-9) into Eq. (3-7a), and completing the integration between points A and C yields

$$\Delta p_{f_{A-C}} = 64\mu\dot{m}_o(H-L)/\pi\rho d_a^4 \tag{3-10}$$

The viscous pressure drop in the wick, between points C and D, can be determined from Darcy's Law [10]

$$\frac{dp}{dx} = \frac{\mu\dot{m}}{\rho KA} \tag{3-11}$$

where K is the wick permeability [11]

$$K = d'^2\varepsilon'^3/[122(1 - \varepsilon')^2] \tag{3-12}$$

and

$$\varepsilon' = 1 - (\pi FNd'/4) \tag{3-13}$$

The crimping factor, F, has the value 1.05 [11]. For an incremental width of wick, dy, the flow area is

$$A = tdy \tag{3-14}$$

and the mass flow rate entering the wick from the artery is

$$\dot{m}_W = \dot{m}'' \, sdy/2 \tag{3-15}$$

We also have a linear variation of the flow rate through the wick, similar to the artery, as follows

$$\dot{m} = \dot{m}_W(1 - 2x/s) \tag{3-16}$$

Substituting, Eqs. (3-3), (3-4) and (3-12)-(3-16) into Eq. (3-11), and completing the integration yields

$$\Delta p_{f_{C-D}} = \mu \dot{q}''s^2(1 + \alpha - L/H)/8\rho K t Q_r \qquad (3-18)$$

Assuming a constant liquid density, the hydrostatic pressure drop between points A and D is

$$\Delta p_{g_{A-D}} = \rho g(H-L) \qquad (3-19)$$

The capillary pumping forces of the wick between points A and D, and A and B, are

$$\Delta p_{s_{A-D}} = 2\sigma(\frac{1}{R_D} - \frac{1}{R_A}), \quad \Delta p_{s_{B-A}} = 2\sigma/R_A \qquad (3-20)$$

since the radius of curvature of the miniscus at B is infinitely large. The capillary pressure difference between B and A is equal to the liquid head difference between the two points

$$\Delta p_{s_{B-A}} = \rho g L \qquad (3-21)$$

Substituting Eq. (3-21) into (3-20) provides the following expression for the capillary pressure difference

$$\Delta p_{s_{A-D}} = 2\sigma/R_D - \rho g L \qquad (3-22)$$

The pumping force will be maximum where $R_D$ is a minimum. For wire mesh, this condition is given by

$$R_{D_{min}} = (\delta + d')/2 \qquad (3-23)$$

At the maximum allowable combustion rate, the capillary pressure difference is a maximum, equal to the sum of the viscous and hydrostatic pressure drops. If we substitute Eqs. (3-3), (3-4a), (3-10), (3-18), (3-22) and (3-23) into (3-7a), and rearrange, the following expression for $\dot{q}''_{max}$ results

$$\frac{\dot{q}''_{max}s^2\mu}{8g\rho^2 KtHQ_r} = \frac{[\frac{4\sigma}{\rho g H(\delta + d')} - 1]}{[1 + \alpha - \frac{L}{H}][\frac{514Kt H^2}{\pi d_a}(1 - \frac{L}{H})^2 + 1]} \qquad (3-24)$$

In order to calculate $\dot{q}''_{max}$, the value of L must be known. The computation of L for a given wick thickness and heat flux is discussed in Ref. 5. The properties of lithium used in the calculations are also summarized in Ref. 5. Two methods were employed for property estimating as follows.

1. Stagnation temperature model. All properties are evaluated at the vapor temperature present outside the wick (which is the stagnation temperature of the heat transport system).

2. Temperature jump model. The temperature difference across the wick, including the evaporative temperature jump, is evaluated [5]. Lithium properties are evaluated at the average wick temperature. This method requires an iterative procedure for each wick heat flux; first assuming an average wick temperature for property evaluation, computing the temperature distribution through the wick, then finding the new average temperature, etc.

## 4. Theoretical Results and Discussion

The theoretical results are presented and discussed in this section. Particular emphasis was placed on the wick configuration to be used in subsequent tests. The dimensions for this standard wick configuration are summarized in Table 1.

TABLE 1

Standard Wick Configuration

| | |
|---|---|
| Height (H-L) | 165 mm |
| Maximum liquid displacement ($L_{max}$) | 73 mm |
| Nominal wick diameter | 56 mm |
| Wick configuration | 2 layers, 100 mesh screen |
| Wick material | Type 316 stainless steel |
| Design temperature | 1200K |

This geometry was fixed by the design of the reactive-heat-pipe combustor that was used for tests with a conventional wick [6].

## 4.1  Self-Priming of Arteries

Table 2 is a summary of the maximum allowable artery dimensions for self-priming the standard wick configuration.  A conservative estimation is shown for the rectangular arteries, where $L_a$ is taken to be large in comparison to $W_a$ (a 2-dimensional artery).

The allowable diameter of the circular artery is about twice as large as for the rectangular artery.  The maximum allowable diameter decreases with increasing temperature, due to the reduction in the surface tension of lithium. The largest possible artery size is desirable, in order to reduce viscous pressure drops.  The sizes shown in Table 2 are reasonable in this regard, and are sufficiently large for convenient fabrication.

TABLE 2

Maximum Artery Sizes for Self-Priming[a]

| TEMPERATURE (K) | DIAMETER OF CIRCULAR ARTERY (mm) | WIDTH OF RECTANGULAR ARTERY (mm)[b] |
|---|---|---|
| 1000 | 1.75 | 0.87 |
| 1100 | 1.71 | 0.86 |
| 1200 | 1.67 | 0.84 |
| 1300 | 1.63 | 0.82 |
| 1400 | 1.59 | 0.79 |

[a] 165 mm vertical self-priming height.  Properties assumed equal to pure lithium.

[b] $L_a$ assumed to be large.

## 4.2 Wick/Artery Performance

### 4.2.1 Influence of Model Assumptions

Table 3 is a summary of the comparison between the two methods of estimating properties in the calculations. The standard wick configuration is considered. The computations provide the maximum allowable heat flux, without wick dryout at point D in Fig. 3, as a function of artery diameter. Wicks with one and two arteries are considered.

### TABLE 3

Comparison of Predictions with the Two Property Models[a]

| ARTERY DIAMETER (mm) | MAXIMUM HEAT FLUX $(kW/m^2)$ | |
| --- | --- | --- |
| | STAGNATION TEMPERATURE METHOD | TEMPERATURE JUMP METHOD |
| One Artery: | | |
| .5 | 73 | 73 |
| 1 | 825 | 828 |
| 2 | 2320 | 2240 |
| 4 | 2615 | 2645 |
| Two Arteries: | | |
| .5 | 148 | 149 |
| 1 | 1960 | 1970 |
| 2 | 8280 | 8550 |
| 4 | 10400 | 10800 |

[a] Standard wick configuration, Table 1, at 1200K.

The results of the two models are nearly the same, with a maximum difference
of 4% for a 4mm artery. Therefore the results of the calculations are relatively
insensitive to the average temperature for property selection for the present
range of heat fluxes.

As the size of the artery increases, the maximum allowable heat flux
increases due to reduced viscous pressure drop in the artery. Eventually a con-
dition is reached, however, where the maximum heat flux becomes relatively
independent of artery size. In this region, the gravitational head and the
viscous pressure drop in the wick itself (in flowing from C to D, Fig. 3) are
the controlling factors. For a required wick height, the hydrostatic pressure
drop cannot be changed; however, the viscous pressure drop in the wick can be
reduced by using more arteries. This is evident by comparing the results for
one and two arteries in the plateau region, comprising the larger artery sizes
in Table 3.

The effect of stagnation temperature on the maximum heat flux is summarized
in Table 4 for a single artery, in the standard wick configuration. This
result also indicates that temperature levels have a relatively minor effect
over the range of interest in this investigation. The effect of the liquid
displacement, L, on the maximum wick power density is also not very large for
the standard configuration. This can be seen from the results given in Table
5.

TABLE 4

Effect of Mean Temperature on Maximum Wick Power Density[a]

| ARTERY DIAMETER (mm) | MAXIMUM HEAT FLUX ($kW/m^2$) | | |
| --- | --- | --- | --- |
| | 1000K | 1200K | 1400K |
| .5 | 67 | 73 | 78 |
| 1 | 753 | 825 | 882 |
| 2 | 2110 | 2320 | 2480 |
| 4 | 2380 | 2615 | 2795 |

[a] One artery, stagnation temperature model, standard wick configuration.

TABLE 5

Effect of Liquid Displacement on Maximum Wick Power Density[a]

| ARTERY DIAMETER (mm) | MAXIMUM HEAT FLUX ($kW/m^2$) | |
|---|---|---|
| | L = 0 | L = 73 mm |
| .5 | 72 | 73 |
| 1 | 810 | 825 |
| 2 | 2270 | 2320 |
| 4 | 2560 | 2615 |

[a] One artery, standard wick configuration, except L as noted, stagnation temperature model.

### 4.2.2  Wick Configuration for the Tests

Test objectives implied a maximum wick power density of 500kW/sq-m.  Due to uncertainties in the uniformity of the reaction rate over the inside surface of the wick, a factor of safety of 8 was specified for the wick pumping capability. This implies a design wick power density of 4000 kW/sq-m.

With this objective, the effect of varying the number and size of arteries was examined for the standard wick configuration.  The stagnation temperature model was used for these calculations, since it is more conservative than the temperature jump model (Table 3).  The results are illustrated in Fig. 4 and summarized in Table 6.  Combining the requirements for self-priming and maximum wick power density, four equally spaced arteries, each having a 1mm diameter, is adequate for the planned test program.  This configuration was selected for the tests.

The use of more arteries would increase pumping capabilities.  However, this increases the problems of artery fabrication and the presence of more arteries would further constrict the heat flow path through the wick.
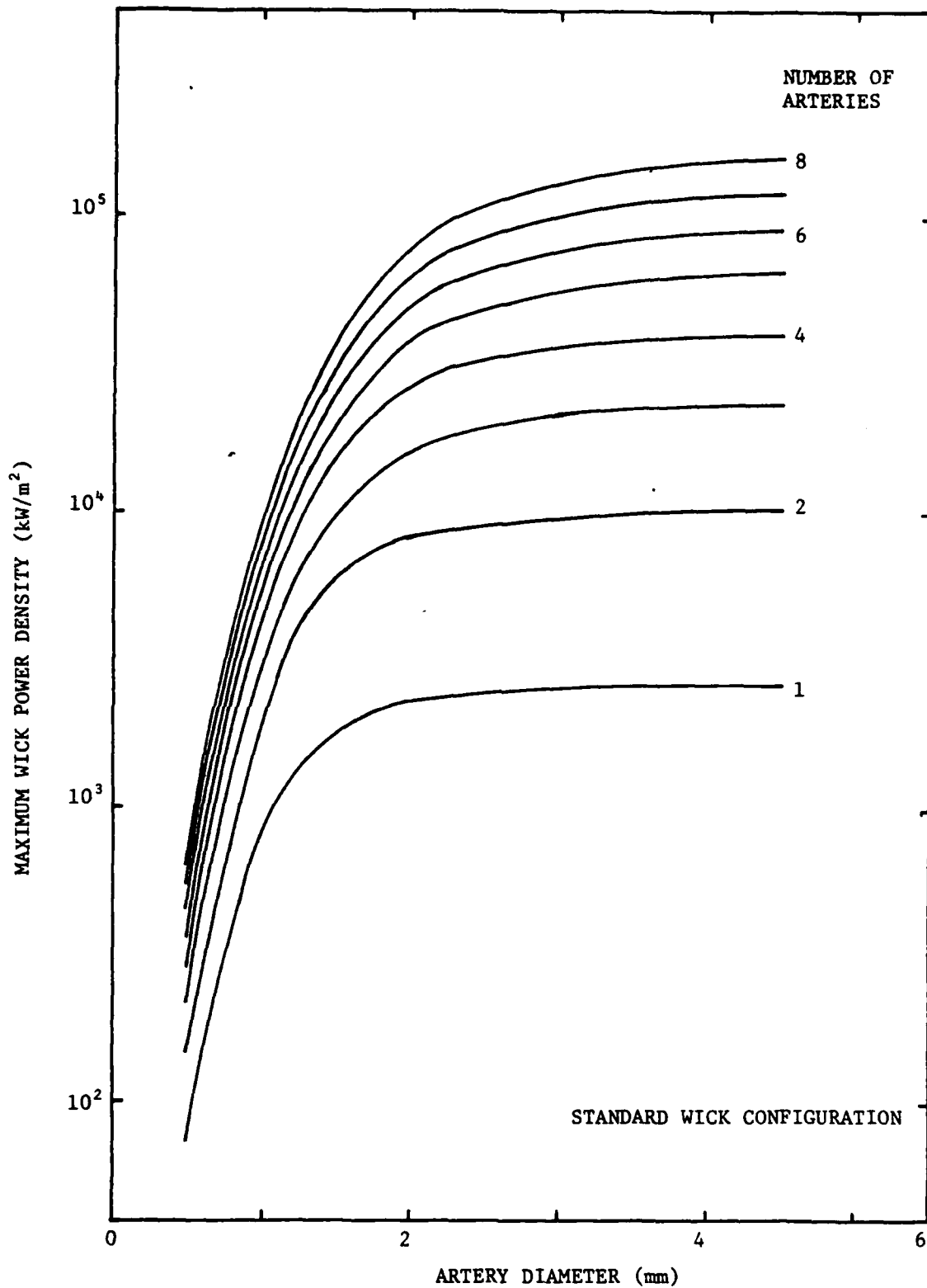
Figure 4  Effect of number and diameter of arteries on
maximum wick power density.

-17-

## TABLE 6

### Effect of Number and Diameter of Arteries
### on Maximum Wick Power Density [a]

| ARTERY DIAMETER (mm) | MAXIMUM HEAT FLUX (kW/m²) | | |
|---|---|---|---|
| | NO. ARTERIES: 2 | 4 | 8 |
| .5 | 148 | 298 | 598 |
| 1 | 1960 | 4315 | 9090 |
| 2 | 8280 | 27290 | 80450 |
| 4 | 10370 | 40790 | 157900 |

[a] Standard wick configuration, stagnation temperature model, 1200K.

At this point, it is useful to compare the arterial wick with the conventional arrangement used in the earlier tests [6]. The analysis of the conventional reactive-heat-pipe is presented by You and Faeth [5]. The maximum heat flux expression is

$$\frac{\dot{q}''_{max} H \mu}{2 g \rho^2 K t Q_r} = \frac{\frac{4\sigma}{\rho g H (\delta + d')} - 1}{(1 + \alpha - \frac{L}{H})(1 - \frac{L}{H})^2} \qquad (4\text{-}1)$$

in the notation of this report.

The performance of these two arrangements is compared in Table 7. The arterial configuration is the present design selection. At each temperature considered in the table, the maximum wick power density of the arterial wick is more than five times higher than the conventional arrangement.

### 4.2.3 Effect of Mesh Size

A final series of calculations examined the effect of mesh size on the four-artery arrangement with the standard wick configuration. The results are illustrated in Fig. 5.

### TABLE 7

#### Comparison of Conventional andArterial Wicks

| Stagnation Temperature (K) | Maximum Heat Flux (kW/m$^2$) | |
|---|---|---|
| | Conventional Wick[a] | Arterial Wick[b] |
| 1000 | 676 | 3930 |
| 1200 | 760 | 4350 |
| 1400 | 833 | 4610 |

[a] Standard wick configuration.

[b] Standard wick configuration, four, 1 mm diameter arteries, stagnation temperature model.

The wick power density reaches an optimum at a certain mesh size. This behavior follows from the counteracting effects of increasing capillary and viscous pressure differences with increasing mesh size. The optimum mesh size of 175 yields only a 28% increase in the maximum wick power density, over the configuration chosen for the tests. Experience with wick fabrication using 100 mesh screen was rather extensive, and the potentially small gain in performance did not warrant a change in wick materials.

## 5. Self-Priming Tests

A series of tests were run in an auxiliary apparatus in order to investigate the self-priming characteristics of the proposed artery designs. The need for these tests was due to the irregular passage shape, compared with those employed in the analysis of self-priming, the use of mesh to form the artery walls (as opposed to a solid tube), as well as uncertainties in the physical properties of the lithium used in present testing.
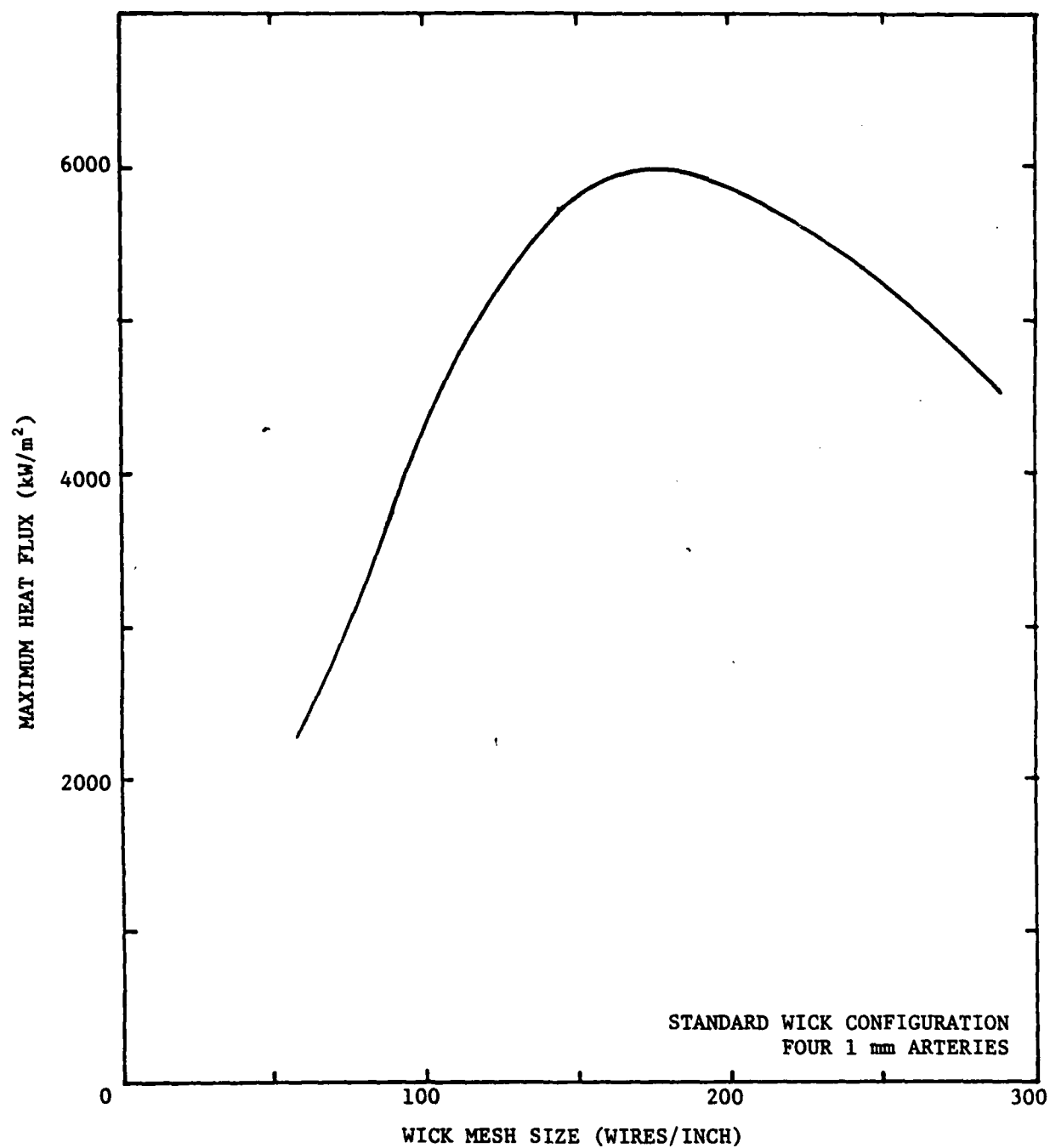
Figure 5  Effect of mesh size on maximum wick power density

## 5.1 Test Apparatus

The self-priming test arrangement is illustrated in Fig. 6. Lithium does not wet new stainless steel parts at low temperatures due to a thin oxide layer present on all such materials. When heated, however, lithium reduces the oxide layer and wets the part [12]. Therefore, it was necessary to simulate the wetting procedure used during combustor operation, which involves heating the wick assembly to 1100-1200K.

The apparatus consists of a cylindrical tube heated with an insulated electrical coil. Four thermocouples were spot-welded to the outside surface of the tube, for temperature monitoring. The upper end of the tube was closed with a cap. A purge flow of argon was provided at the top of the tube in order to prevent contamination of the lithium with air.

The test assembly consisted of a wick segment, 400 mm long and 40 mm wide, containing one artery. The wick/artery segment was spot-welded to a rod, which held the segment vertical and provided a means of removing the assembly following a test. The bottom of the segment was placed in a pool of lithium which supplied the liquid for self-priming.

The wick was constructed of two layers of 100 mesh type 316 stainless steel woven wire cloth. The arteries were constructed by deforming the outer layer of mesh with a die, so that the passage was between the two layers of screen. The two layers of screen were spot-welded together.

The test procedure involved purging the tube with argon and then adding solid lithium, which when melted would form the pool. The wick/artery segment was then placed in the tube, resting on the bottom. The system was heated to 1140K and allowed to stand for approximately one-half hour. The heaters were then turned off and the system was allowed to cool. Before the pool of lithium solidified, the wick/artery segment was raised out of the liquid so that it could be readily removed for inspection when cooling was complete.

## 5.2 Results and Discussion

The results of the self-priming tests are summarized in Table 8. The first configuration only primed to 140 mm and was unsatisfactory. This artery was somewhat oversized, and due to relatively crude dies, the crossectional area of the artery varied along the length of the segment. The maximum artery dimension was also larger than a circular artery of the same crossectional area.

The second test involved the use of better dies, achieving the desired dimensions. However, the self-priming height was only slightly above the required design height of 165 mm. This was judged to be an insufficient safety margin for the design due to potential uncertainties in fabrication of the entire wick assembly.
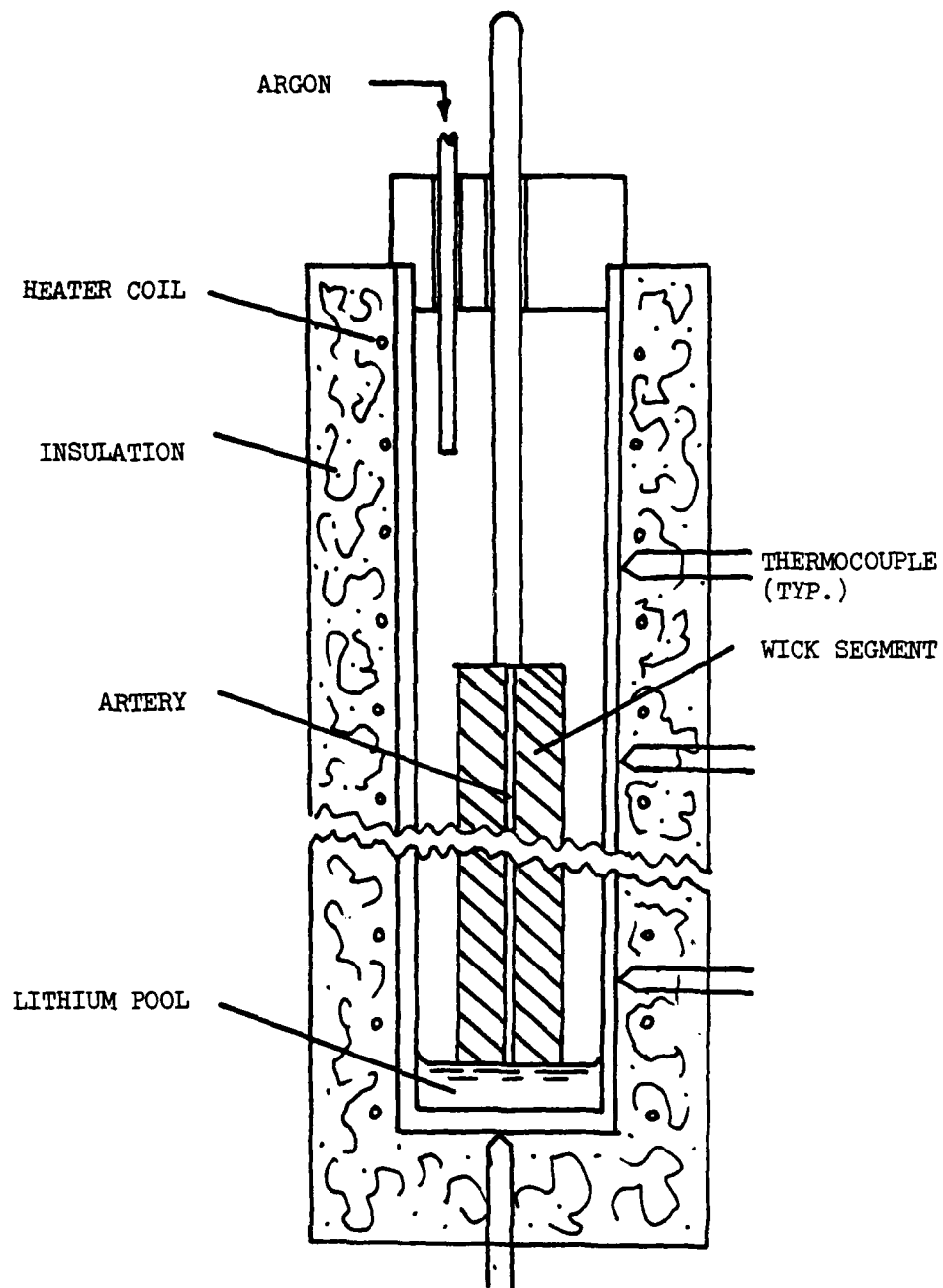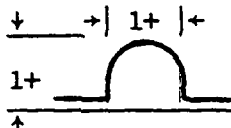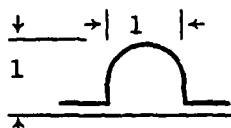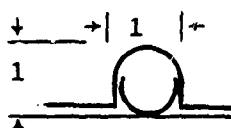
Figure 6   Sketch of self-priming evaluation apparatus

The third test arrangement employed a half-artery insert to provide a more circular passage. This arrangement yielded a self-priming height of 304 mm, compared to the predicted height of 280 mm for a circular artery of 1 mm ID at the temperature levels of the tests.

Figure 7 is a photograph of this assembly following the test. The wick itself is primed nearly to the top of its 400 mm length. The top does not prime since this region was cooler and did not provide conditions where the surface was properly prepared for wetting by lithium. The wick forming the artery passage is not wetted beyond the height to which the artery is primed. This illustrates the importance of complete self-priming for the present design, since unwetted portions of the wick would be rapidly attacked by $SF_6$ at typical combustor operating conditions.

TABLE 8

Summary of Self-Priming Test Results

| TEST | GEOMETRY[a] | SELF-PRIMING HEIGHT (mm) |
|------|-------------|--------------------------|
| 1 |  | 140 |
| 2 |  | 178 |
| 3 |  see note b | 304 |

[a] Lines represent outer surface of mesh, dimensions in mm.

[b] A one-half artery insert was spot-welded to the outer surface of the inner layer of screen in this configuration.
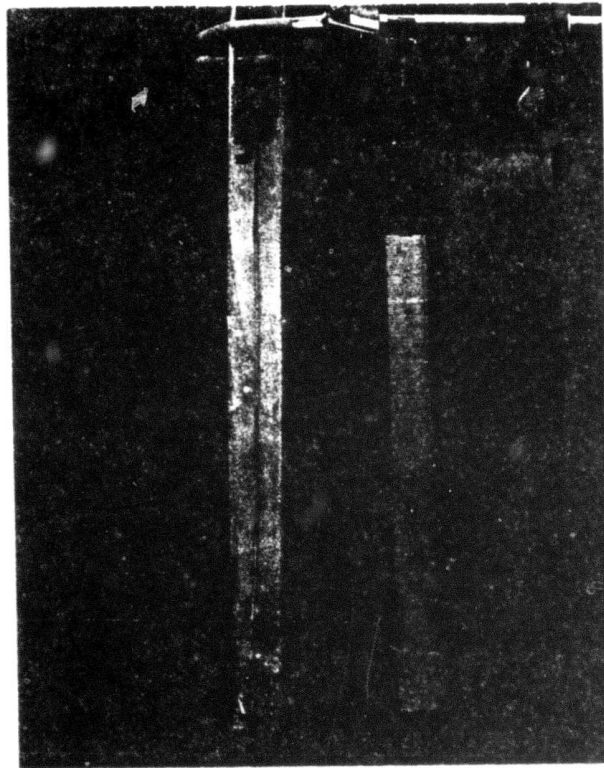
Figure 7  Photograph of the Wick/Artery Segment after Test 3.

## 6.  Reactive-Heat-Pipe Combustor Tests

### 6.1  Test Apparatus

The apparatus used to test the arterial wick arrangment was identical to
the design employed in earlier reactive-heat-pipe tests [6]. Only a brief
description will be presented here, complete details may be found in Ref. 6.

Crossectional sketches of the side and end views of the combustor appear
in Figs. 8 and 9. The design is summarized in Table 9. The only change in
the system from the earlier tests [6], involved the use of arterial wick assemblies.
The wick configuration employed four arteries having the same geometry as Test 3
of the self-priming tests. The arteries were equally spaced around the periphery
of the wick. A photograph of an arterial wick assembly prior to installation
in the combustor appears in Fig. 10. The combustor employed two injector/wick
assemblies.

The combustor is filled to its centerline with fuel. The upper half of the
combustor acts as the load heat exchanger while the lower half acts as a fuel-
product storage region. Heat is transferred from the combustor by convection
and radiation to the surrounding test cell. The rate of heat loss can be
varied by changing the position of movable radiation shields over the heat
exchanger area.

The sulfurhexafluoride flows independently to the two injector/wick
assemblies. The flow rate to each injector is monitored by measuring the upstream
pressure on two critical flow orifices. The flow is varied by varying the pressure
upstream of the orifices with pressure regulators.

The combustor is ignited by heating the system with electrical coils located
under the insulation around the body of the combustor. These coils also facilitate
heating the combustor when fuel is added or combustion products are removed [6].
The combustor is operated in a batch mode.

Combustor temperatures are monitored with chromel-alumel thermocouples
spot-welded to the surface. The temperatures are recorded on several Leeds and
Northrup Speedmax H, Type S multipoint recorders. Calibration, wick priming
and degassing procedures were the same as in earlier tests [6].

TABLE 9

Design Summary of Reactive-Heat-Pipe Employing Arterial Wicks

---

| | |
|---|---|
| Fuel Loading | 6 kg |
| Energy Content[a] | 75 kW-hr[a] |
| Maximum Power | 15 kW |
| Dimensions | 273 mm diameter x 521 mm long (uninsulated) |
| Number of Injectors | 2 |
| Wick Material | 2 layers, 100 x 100 mesh, type 316 stainless steel woven wire cloth |
| Wick Diameter | 56 mm |
| Active Wick Height[b] | 160 mm |
| Wick Power Density[c] | 250 kW/m$^2$ |
| Artery Configuration | 4 per wick, 1 mm diameter |
| Heat Exchanger | Radiative |
| Baffle Passage Dimensions | 23 mm wide x 380 mm long, passage ends 25 mm above liquid surface |
| Heat Exchanger Power Density | 92 kW/m$^2$ (maximum) |
| Start System | Electrical Heaters |

---

[a] Based on 12.46 kW-h/kg of fuel [8].

[b] Distance from outside liquid surface to top of wick.

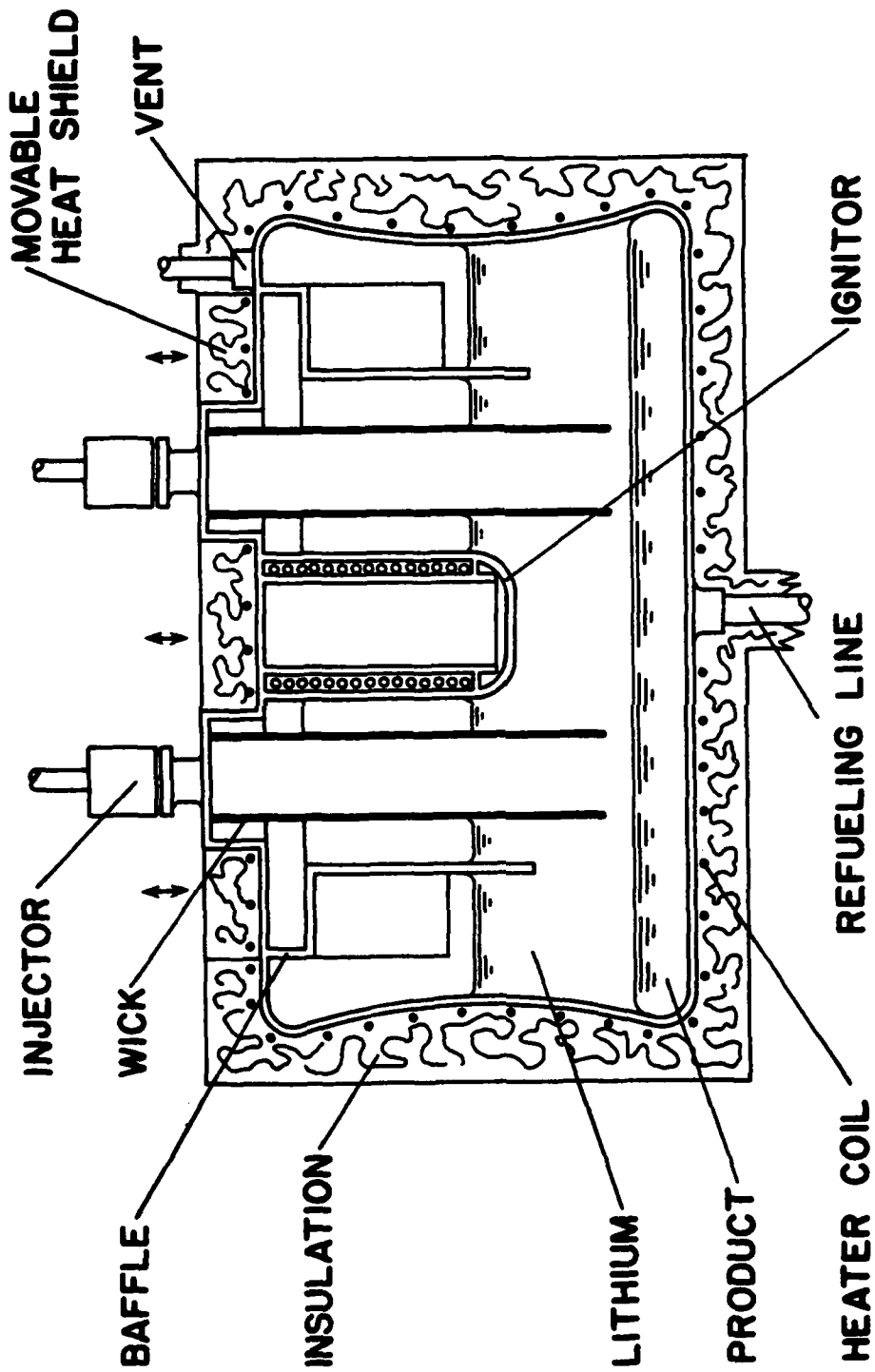[c] Both wick assemblies operating at full combustor power.

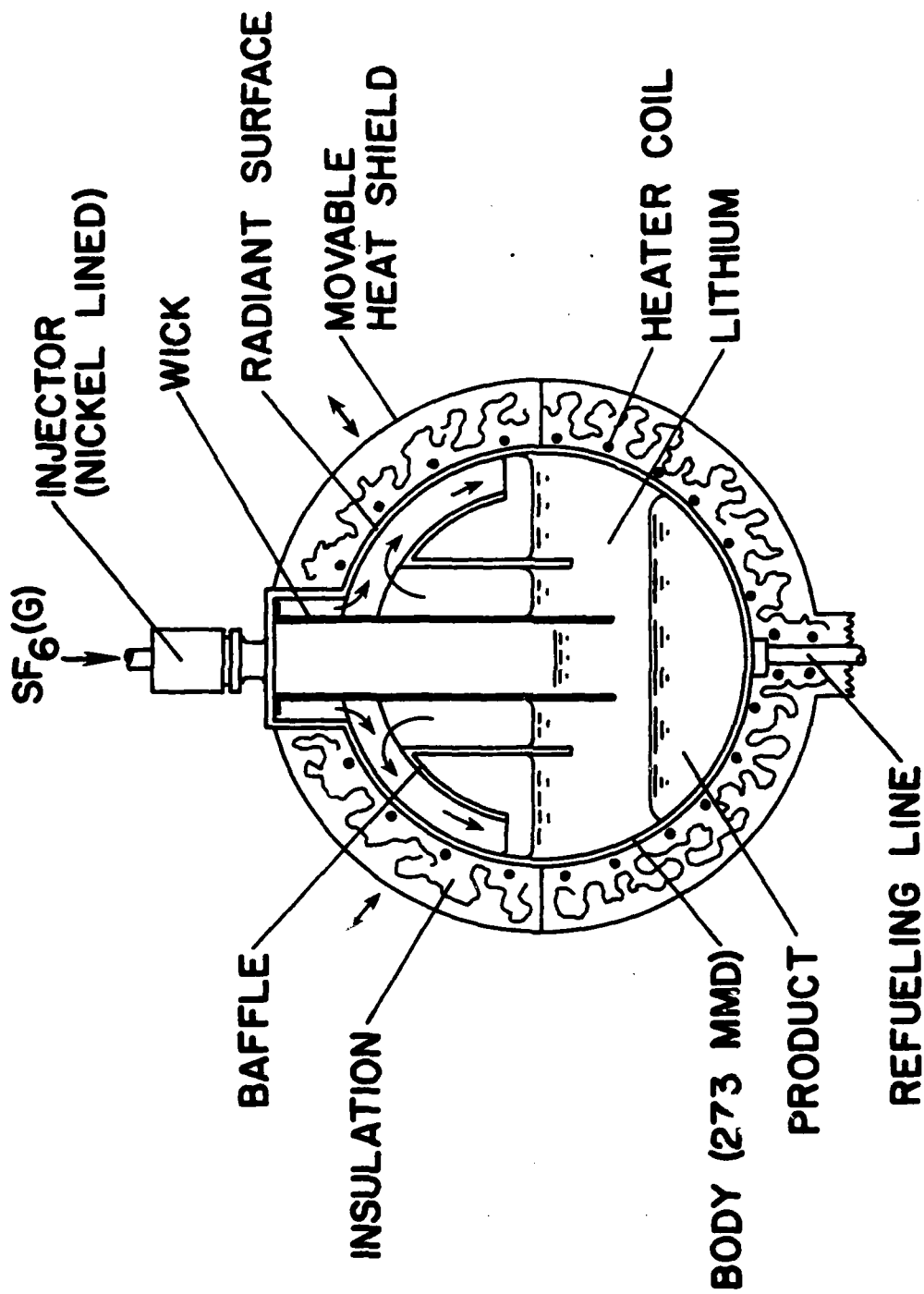Figure 8   Side View of the Experimental Reactive-Heat-Pipe Combustor

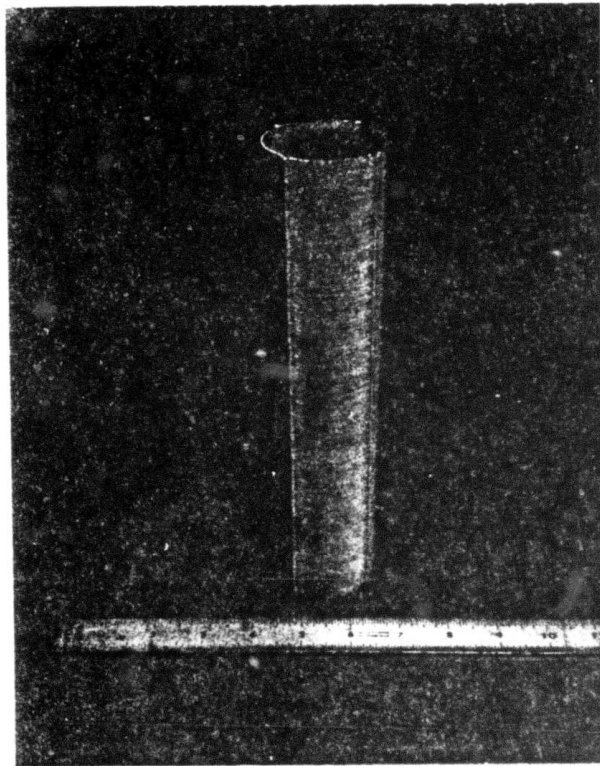Figure 9  End View of the Experimental Reactive-Heat-Pipe Combustor

Figure 10   Photograph of an arterial wick assembly
prior to installation in the combustor.

## 6.2 Test Results and Discussion

The objectives of the combustor test were to demonstrate the operation of arterial wick assemblies, and to determine the maximum wick power density without wick burnout. The maximum possible wick power density that could be considered was 500 kW/m$^2$. This corresponds to the combustor running at full power on one injector/wick assembly.

The major results of the test are summarized in Table 10. This test ran for 2.5 hours, and was terminated since both wicks had exceeded their maximum power densities and had given indication of burnout. This was the sixth test with the combustor, with total operating time of the unit was 18.6 hours, following the test.

TABLE 10

Summary of Arterial Wick Reactive-Heat-Pipe Combustor Test[a]

| | |
|---|---|
| Duration (h) | 2.5 |
| Maximum Power (kW) | 14 |
| Maximum Wick Power Density[b] (kW/m$^2$) | |
|     Left Wick | 440 |
|     Right Wick | 312 |
| Maximum Flow Power Density[b] (kW/m$^2$) | |
|     Left Wick | 5030 |
|     Right Wick | 3565 |
| Maximum Wall Temperature (K) | 1175 |

[a] This was the sixth test with this combustor. The other tests are described in Ref. 6. The total operating time of the combustor following this test was 18.6 h.

[b] Power density when wick burnout was detected.

Combustor operating conditions during the test are illustrated in Figs. 11-14. The combustor was ignited at 920K and brought to operating temperatures. This was done relatively slowly so that satisfactory operation of the system could be verified prior to running at high power levels.

Once operating temperatures were reached, the combustor power level was increased in steps to a full power condition. Each power setting was maintained for about 10 minutes so that stable operation was assured before the next power increase was undertaken. Combustor wall temperatures were maintained relatively constant, the power level was varied by moving the radiation shields. In this period, the injectors were equally loaded, Fig. 13, finally reaching the original design wick power density of 250 kW/m$^2$.

The left injector was then tested at higher power levels, in steps, while reducing the flow rate to the right injector in order to maintain a constant wall temperature at full power operation. After about ten minutes of operation at a wick power density of 440 kW/m$^2$, a local hot spot was observed on the injector riser. This was also accompanied by a rapid increase in combustor pressure. It was assumed that wick burnout had occurred and the combustor was immediately brought to idle. At this point the hot spot disappeared.

The test continued using the right injector with the left injector remaining at idle. In this case a local hot spot and a rapid rise in combustor pressure was observed at a power density of 312 kW/m$^2$. The combustor was then shut down and the contents were transferred to the product storage tank, using the dump procedure described in Ref. 6. After cooling, the combustor was opened for inspection.

Aside from the rapid pressure spike noted when the hot spot appeared, pressures in the reaction space of each wick assembly were normal, cf.Fig. 14. As power levels increase and decrease, pressures vary accordingly in response to the varying temperature levels, and thus vapor pressure levels, on the inside surface of the wick [4].

Figure 15 is a photograph of the wick assemblies following the test. The right wick had an oval shaped hole about 8 mm long and 5 mm wide, located about 20 mm from the top of the wick and 12 mm from the nearest artery. The hole in the left wick was larger, 12 mm by 7 mm, located about 20 mm from the top of the wick, about half-way between the arteries. The remainder of each wick was in good condition with no evidence of damage from the hot spots. Reduced damage in comparison to earlier wick burnout tests was the result of earlier recognition of burnout and reduction of oxidizer flow rates.

If reaction rates were uniform, the observed conditions at failure should not have been severe. It appears that substantial reaction rate nonuniformities are present in this design, with the bulk of the reaction concentrated in the upper portion of the wick at high oxidizer flow rates. The fact that the holes did not appear at the very top of the wick is not surprising, since this region is quenched to some degree by heat loss from the injector area.
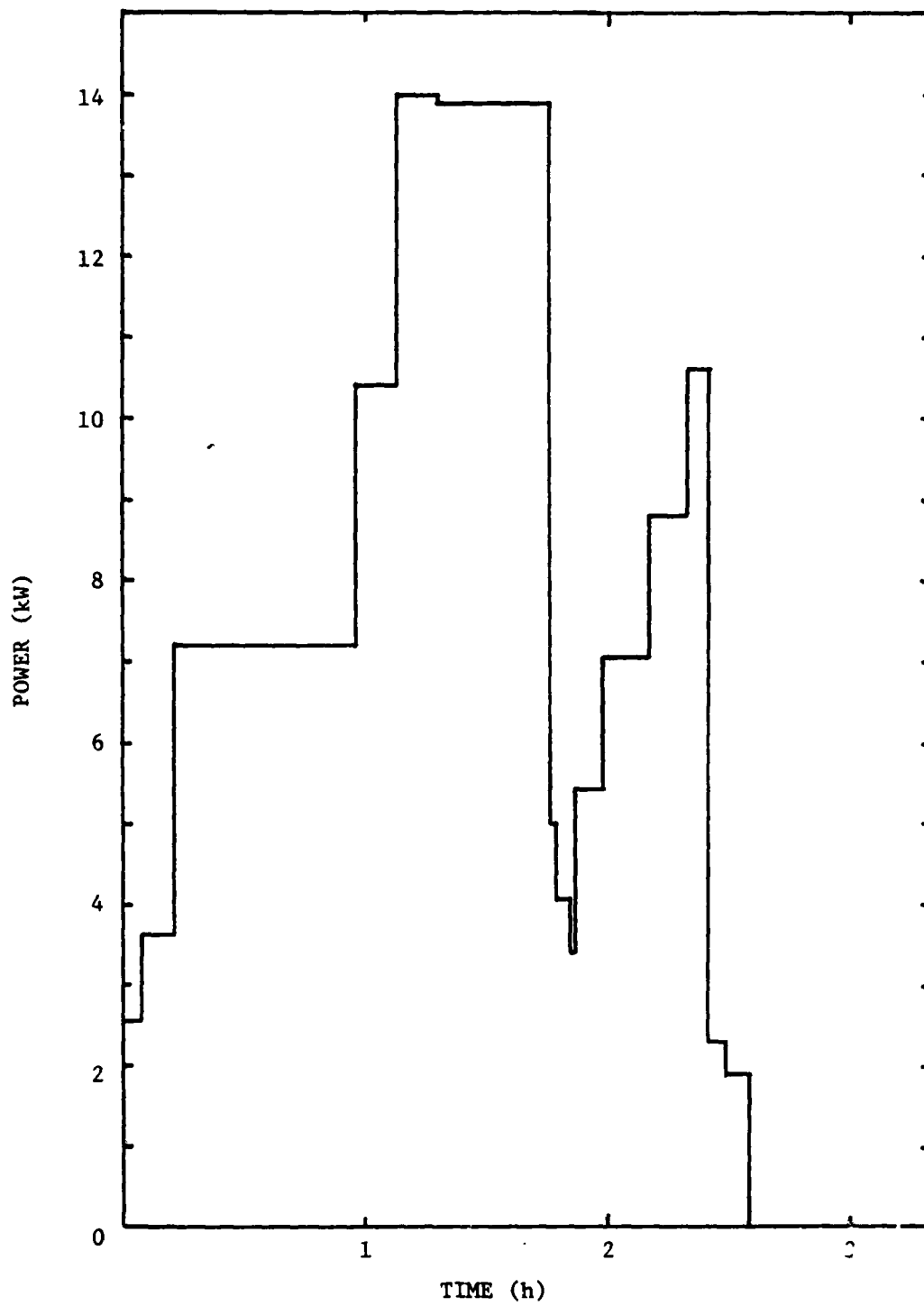
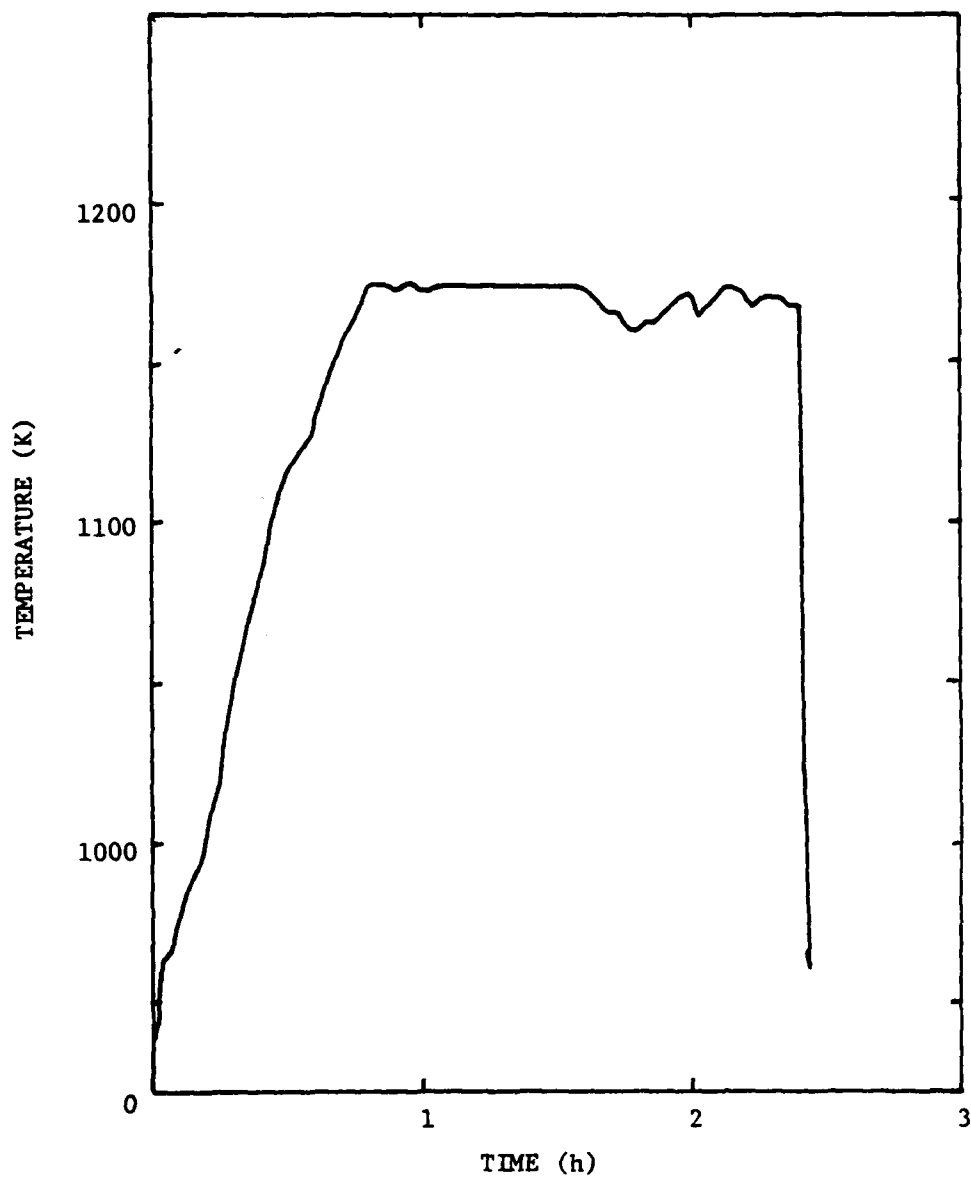Figure 11   Total power variation during the test.

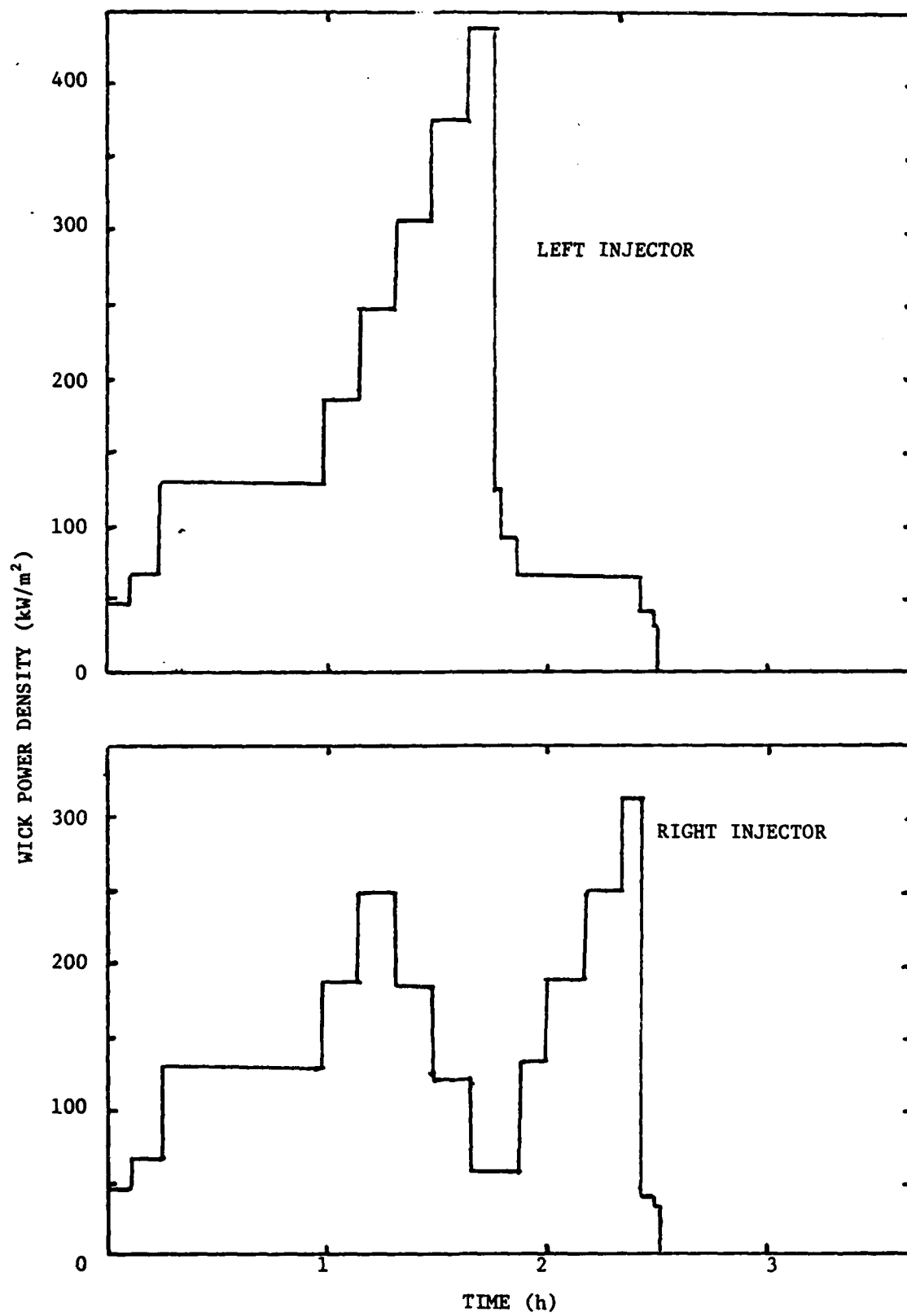Figure 12   Condenser wall temperature during the test.
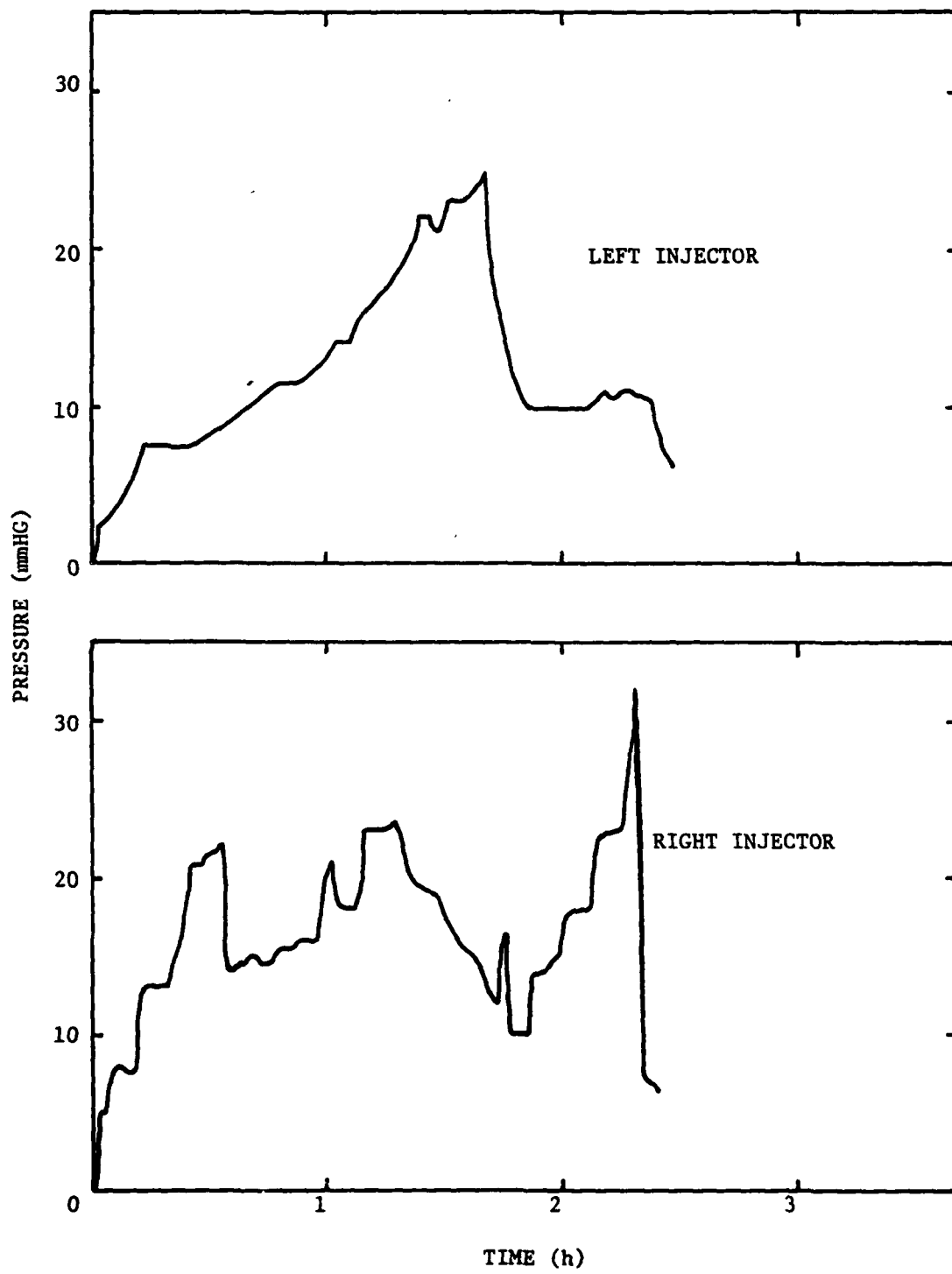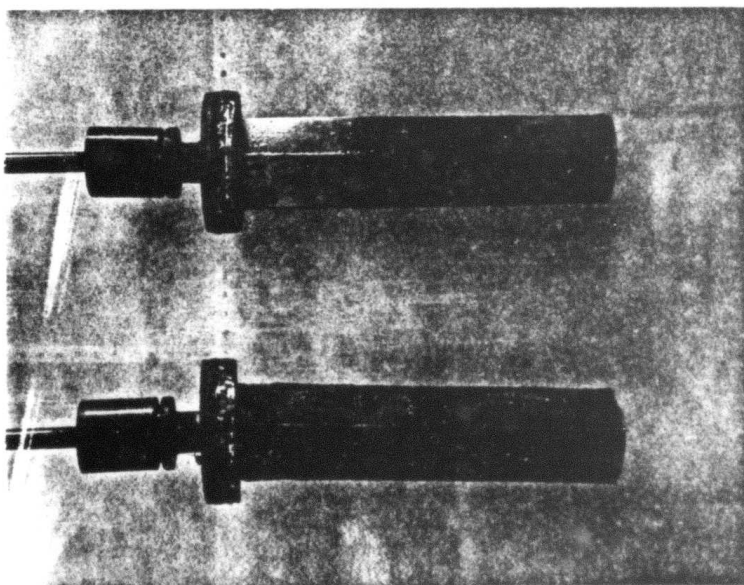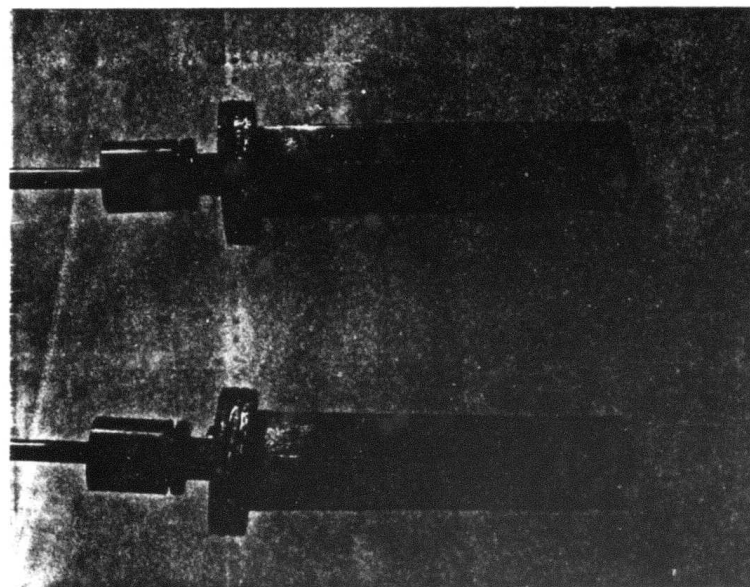
Figure 13  Wick power densities during the test.

Figure 14  Injector pressures during the test.

Left Wick    Right Wick

BAFFLE SIDE



Left Wick    Right Wick

IGNITOR SIDE

Figure 15   Photographs of wick assemblies after the test.

The relation between the pressure spike noted at the time of burnout, and burnout itself is not understood at this time. A sudden increase in wick temperature should be accompanied by an increase in pressure, as noted earlier. However, wick burnout only yielded high temperatures in a limited area, and the mechanism for the entire reaction zone increasing in pressure is not clear.

Another explanation for the pressure rise is that the injector flow was partially deflected by product condensed on the top of the reaction zone. Periodic pressure disturbances of this type have been observed during most tests with wick-type combustors. The cycle involves gradually decreasing temperatures near the injector, accompanied by an increase in the indicated combustor pressure (taken to represent an increased pressure drop across the injector). This is followed by a period of increased temperatures in the injector area and normal combustor pressures for the operating condition. These events suggest the build-up of a product layer along the top surface of the combustor, which insulates the metal and also interferes with the flow through the injector. The layer then reaches a critical thickness and drips-off, reducing both the thermal and flow resistance. Product condensate accumulates again and the cycle repeats itself.

If the flow through the injector is impeded, the gas jet leaving the injector could be deflected toward the wick surface. This would result in high transport, and thus reaction, rates at the stagnation point where the flow strikes the wick, resulting in the local burnout observed in these tests. High flow rates would be more critical, since the jet penetrates further into the reaction space at these conditions, and stagnation point transport rates increase with increasing local velocities.

The correction for either of these explanations would involve reducing the aspect ratio of the wick. Stated another way, the modification would require reduced flow power densities. This would reduce nonuniformity since more area would be available for mixing. If the jet were deflected, the distance to the wick would also be greater, reducing stagnation point transport rates. If deflection is the major problem, modification of the injector, perhaps extending the tip further into the reaction space, would also be helpful.

Some noncondensibles were observed in the heat transport system during the test, although their presence did not limit maximum power capabilities. Condenser wall temperature distributions are illustrated in Figs. 16 and 17. The axial distributions shown in Fig. 17 particularly illustrate noncondensible effects. When only the left injector was operating, the vapor flow pumps the noncondensibles to the right side of the combustor, resulting in low temperatures in this region. The directions are just reversed when only the right injector is operating.
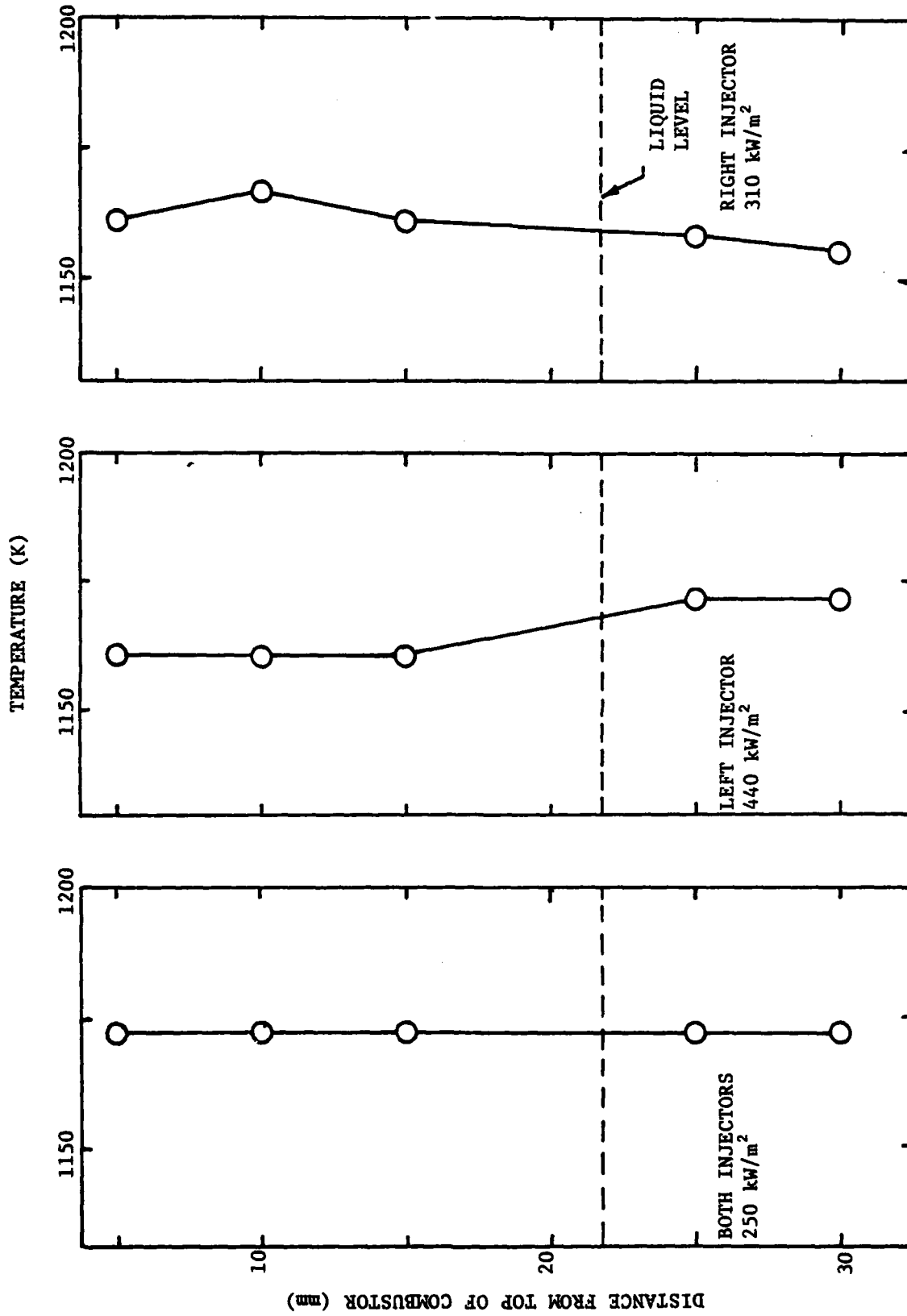
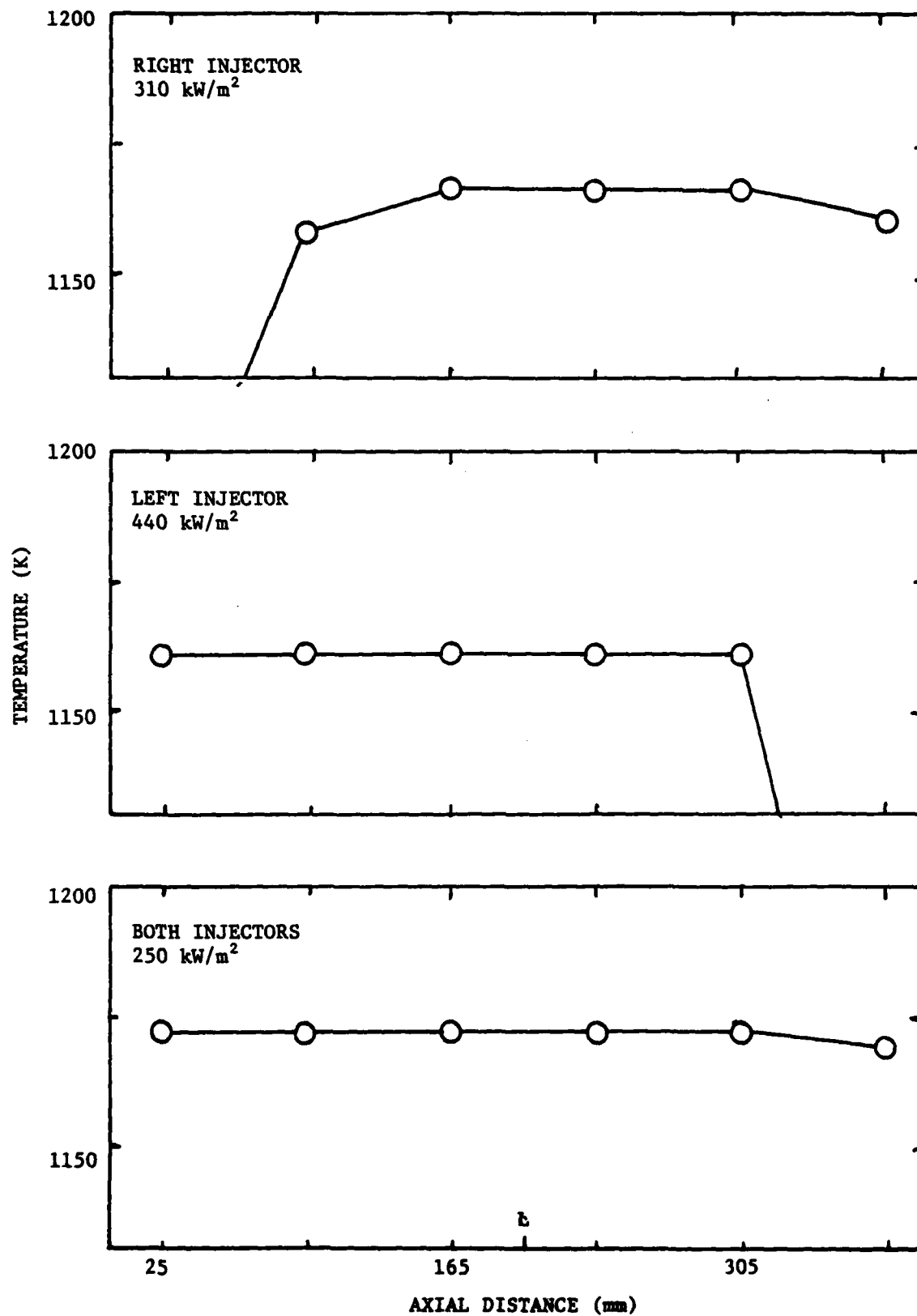Figure 16  Circumferential wall temperature distributions

-38-



Figure 17  Axial wall temperature distributions

## 7. Conclusions

The theoretical results indicate that arterial wicks show good potential for increasing the wick power density of reactive-heat-pipe combustors. Predicted wick power densities are in the range of $MW/m^2$, which would provide relatively compact wick arrangements.

The test results verified the self-priming predictions, when the arteries were accurately fabricated.

The wick power densities achieved during the present tests were only slightly higher, at burnout, than earlier results with conventional wicks [6]. This occurred even though the present wicks had almost 8 times the pumping capability of the conventional design. The result suggests that burnout is a very nonlinear event, which when started can exceed the pumping capabilities of practical wick designs. Deflection of the jet toward the wick is the most likely event of this type, although nonuniform combustion confined over the upper portions of the wick is probably a contributing factor.

The design adjustment required to overcome nonuniform combustion involves providing a greater distance between the injector and the wick. This can be accomplished by using lower wick aspect ratios. Modification of the injector to reduce the possibility of jet deflection would also be helpful. If proper cooling can be maintained, extending the injector into the reaction space should also help, since the product condensate would be directed more along the line of flow of the jet with less potential for blockage of the injector passage.

All other aspects of the test were satisfactory. The levels of noncondensibles were low and good condenser action was achieved. Variable load operation with different power levels on each wick was demonstrated with no difficulty. Filling and dumping procedures were routine. Aside from the small holes in the wick, which were inevitable due to the objectives of the test, all combustor components were in excellent condition following the test.

1. Faeth, G. M., Kuo, K. K., and Olson, D. R., "A Study of a Liquid Metal Thermal Energy Source", Final Report, Contract No. N00600-73-C-0113, Mechanical Engineering Department, The Pennsylvania State University, University Park, PA, September 1973.

2. Blakeslee III, T. R., Groff, E. G., Faeth, G. M., and Olson, D. R., "A Study of a Liquid Metal Thermal Energy Source", Annual Report, Contract No. N00600-74-C-0033, Mechanical Engineering Department, The Pennsylvania State University, University Park, PA, September 1974.

3. Groff, E. G., and Faeth, G. M., "Characteristics of a Steadily Operating Metal Combustor", Technical Report, Contract No. N00600-74-C-0033, Mechanical Engineering Department, The Pennsylvania State University, University Park, PA, August 1976.

4. Blakeslee III, T. R., and Faeth, G. M., "Combustion of a Liquid Metal from a Wick", Technical Report, Contract No. N00600-74-C-0033, Mechanical Engineering Department, The Pennsylvania State University, University Park, PA, May 1977.

5. You, H-Z, and Faeth, G. M., "A Reactive-Heat-Pipe for Combined Heat Generation and Transport", Technical Report, Contract No. N00600-74-C-0033, Mechanical Engineering Department, The Pennsylvania State University, University Park, PA, December 1977.

6. Alstadt, R. H., and Faeth, G. M., "An Investigation of Wick-Type Metal Combustors", Technical Report, Contract No. N00600-74-C-0033, Mechanical Engineering Deparment, The Pennsylvania State University, University Park, PA, December 1977.

7. Avery, J. F., and Faeth, G. M., "Combustion of a Submerged Gaseous Oxidizer Jet in a Liquid Metal", Fifteenth Sumposium (International) on Combustion, pp. 501-512, The Combustion Institute, Pittsburgh, PA, 1974.

8. Groff, E. G., and Faeth, G. M., "Steady Metal Combustor as a Closed Thermal Energy Source", J. Hydronautics, Vol. 12, No. 2, pp. 63-70, April 1978.

9. Faeth, G. M., Groff, E. G., You, H-Z, Alstadt, R., and Icenhower, D., "A Reactive-Heat-Pipe for Combined Heat Generation and Transport", AIAA Paper No. 78-440, Proceedings of 3rd International Heat Pipe Conference, pp. 316-326, May 1978.

10. Dunn, P. D., and Reay, D. A., Heat Pipes, 1st ed., Pergamon Press, New York, 1975.

11. Ferrill, J. K., Winston, H. H., and Davis, R., "Heat Pipe Wick Properties and Performance", Department of Chemcial Engineering, North Carolina State University, Raleigh, N. C., October 1973.

12. Mausteller, J. W., Tepper, F., and Rodgers, S. J., Alkali Metal Handling and Systems Operating Techniques, pp. 154-155, Gordon and Breach, New York, 1967.

# Distribution and Addressee Listing

| Addressee | Copies |
|---|---|
| Director<br>Advanced Research Projects Agency<br>Architect Building<br>1400 Wilson Blvd.<br>Arlington, VA 22209 | 3/0 |
| Officer in Charge<br>David W. Taylor<br>Naval Ship Research and Development Center<br>Annapolis Laboratory<br>Annapolis, Maryland 21402<br>Attn: Mr. S. Cox, Code 2724 | 9/1 |
| CDR C. E. Moore, OPNAV 233<br>Chief of Naval Operations, Off of the<br>Room 5E577 Pentagon<br>Washington, D. C. 20301 | 1/0 |
| TACTEC<br>Battelle Columbus Laboratories<br>505 King Avenue<br>Columbus, Ohio 43201 | 1/0 |
| Dr. Eugene C. Gritton<br>The Rand Corporation<br>1700 Main Street<br>Santa Monica, CA 90406 | 5/0 |